Quantum fluctuations in antiferromagnets of the BX_2 family

1996 J. Phys.: Condens. Matter 8 1811

(http://iopscience.iop.org/0953-8984/8/11/024)

J. Phys.: Condens. Matter **8** (1996) 1811–1830. Printed in the UK

Quantum fluctuations in antiferromagnets of the BX_2 family

E Rastelli and A Tassi

Dipartimento di Fisica dell'Universitá and INFM, 43100 Parma, Italy

Received 13 October 1995, in final form 16 January 1996

Abstract. The hexagonal antiferromagnet, convenient for describing magnetic compounds of the type BX_2, where B is a magnetic ion and X a halogen, is characterized by having an in-plane exchange interaction $J_\perp$ much stronger than the out-of-plane exchange interaction $J_\parallel$. The interest in the class of BX_2 compounds arises because they are expected to manifest some features peculiar to the triangular antiferromagnets. In particular, we intend to investigate the existence of possible planar phases supported by quantum fluctuations when an external magnetic field is applied perpendicular to the c axis. We find that a planar phase is stable for sufficiently small interplane coupling and small single-ion easy-axis anisotropy, whereas an umbrella phase would be expected on the basis of the classical approximation.

1. Introduction

The behaviour of hexagonal antiferromagnets (HAF) in an external magnetic field is currently being investigated, but many questions await an answer. The HAF model is suitable for describing ABX_3 and BX_2 compounds where A is an alkali element, B a magnetic ion and X a halogen [1]. The magnetic ions are localized on antiferromagnetic chains along the c axis and form a triangular antiferromagnet (TAF) in the c plane. The basic difference between ABX_3 and BX_2 compounds is in the value of the ratio between $J_\parallel$ (the NN intrachain coupling) and $J_\perp$ (the NN interchain coupling). One has $J_\parallel \gg J_\perp$ in ABX_3 and $J_\parallel \ll J_\perp$ in BX_2 compounds [2], so characteristic features of 1D antiferromagnetic chains and of 2D triangular antiferromagnets may be found in ABX_3 and BX_2 compounds, respectively. For instance, experimental support to the Haldane conjecture [3] was achieved via inelastic neutron scattering from $CsNiCl_3$, a member of the ABX_3 family [4]. It is worth noticing, however, that the experimental data on $CsNiCl_3$ may also be understood as due to anharmonic magnon–magnon interactions peculiar to non-collinear quasi-1D spin systems [5]. An interesting debate is still open. In contrast, the peculiar phenomenology of the TAF [6] model is expected to be observed for BX_2 compounds when an external magnetic field is applied in the c plane. We recall that quantum fluctuations stabilize a *planar* configuration in the TAF model with the spins spiralling in a plane containing the magnetic field even though an *umbrella* configuration with its axis along the magnetic field direction has the same energy as the planar configuration in the classical approximation [7]. This interesting quantum effect is prevented in the ABX_3 antiferromagnets because of the strong intrachain coupling $J_\parallel$ that makes these compounds similar to independent antiferromagnetic chains rather than to triangular antiferromagnets. The case of $CsCuCl_3$ is unique since the strong intrachain interaction is ferromagnetic, so any chain behaves like a

0953-8984/96/111811+20$19.50

single spin at low enough temperature. The TAF phenomenology was indeed experimentally observed [8] and theoretically justified [9]. This possibility is prevented when the strong intrachain coupling is antiferromagnetic—as is mostly the case for the ABX_3 compounds. In contrast, because of the strong interchain coupling $J_\perp$ and the small single-ion anisotropy, the BX_2 compounds are expected to behave like triangular antiferromagnets, since the small intrachain coupling $J_\parallel$ makes these systems similar to a stacking of nearly independent triangular antiferromagnets. Indeed the difference between the umbrella and the planar configuration energies in the classical approximation is of order $-J_\parallel H^2$. On the other hand one expects to find that the difference between the zero-point-motion energy of the umbrella and the planar configuration of the HAF is of order $+J_\perp H^2/S$ on the basis of what occurs in the TAF model [7]. As a consequence we expect that the competition between classical and quantum contributions to the ground-state energy will be found to play a significant role in the BX_2 family. Notice that the quantum effect decreases as S increases, but for any reliable value of S the quantum effect is far from being negligible for BX_2 compounds where $J_\perp \gg J_\parallel$.

In this paper we investigate the possibility of planar spin configurations supported by quantum fluctuations when an external magnetic field is applied in the c plane with and without single-ion easy-axis anisotropy. The HAF model with small interlayer coupling and small anisotropy is suitable for describing VBr_2 (a BX_2 compound with $S = 3/2$) for which elastic neutron scattering data exist [2].

In section 2 we evaluate the minimum-energy configuration in the classical approximation. In section 3 we evaluate the magnon frequencies and in section 4 the zero-point-motion energy for the planar (P) and umbrella (U) configurations. In section 5 the consequence of quantum fluctuations for the Bragg peaks is considered in order to compare our results with experiment. Section 6 is devoted to conclusions and comments.

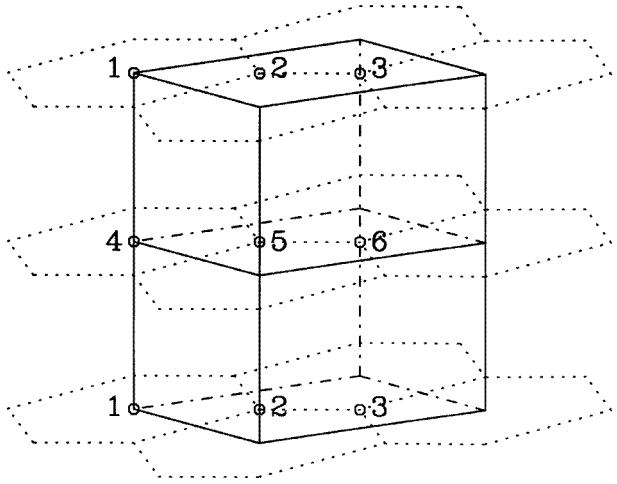

Figure 1. The magnetic cell of the hexagonal antiferromagnet (HAF).

2. The minimum-energy configuration in the classical approximation

The Hamiltonian model that we consider reads

$$\mathcal{H} = J_{\parallel} \sum_{i,\delta_{\parallel}} \boldsymbol{S}_i \cdot \boldsymbol{S}_{i+\delta_{\parallel}} + J_{\perp} \sum_{i,\delta_{\perp}} \boldsymbol{S}_i \cdot \boldsymbol{S}_{i+\delta_{\perp}} - g\mu_B H \sum_i S_i^x + D \sum_i (S_i^z)^2 \tag{2.1}$$

where $J_{\parallel}$ is the NN intrachain coupling, $J_{\perp}$ is the NN interchain coupling, $\boldsymbol{\delta}_{\parallel}$ is a vector joining the site i with its two out-of-plane NN at $(0, 0, \pm c)$ and $\boldsymbol{\delta}_{\perp}$ is a vector joining the site i with its six in-plane NN at $(\pm a, 0, 0)$, $(\pm a/2, \pm\sqrt{3}a/2, 0)$. g is the Landé factor, μ_B is the Bohr magneton, H is the external magnetic field applied along the x direction and $D < 0$ is the single-ion easy-axis anisotropy. The magnetic cell of the HAF model is shown in figure 1.

In the classical approximation the spins are represented by classical vectors of magnitude S, so the energy of the model (2.1) is a function of the polar angles θ_s and azimuthal angles ϕ_s of the six spins of a unit cell, where $s = 1, 2, 3$ labels the spins in a layer and $s = 4, 5, 6$ labels the spins in the adjacent layer. Spins labelled 1 and 4, 2 and 5, 3 and 6 are NN along the c axis, respectively.

The reduced energy reads

$$\begin{aligned} e_0 = \frac{E_0}{2J_{\perp}NS^2} &= \frac{1}{2}\big[\sin\theta_1\sin\theta_2\cos(\phi_1-\phi_2) + \cos\theta_1\cos\theta_2 \\ &+ \sin\theta_2\sin\theta_3\cos(\phi_2-\phi_3) + \cos\theta_2\cos\theta_3 + \sin\theta_3\sin\theta_1\cos(\phi_3-\phi_1) \\ &+ \cos\theta_3\cos\theta_1 + \sin\theta_4\sin\theta_5\cos(\phi_4-\phi_5) + \cos\theta_4\cos\theta_5 \\ &+ \sin\theta_5\sin\theta_6\cos(\phi_5-\phi_6) + \cos\theta_5\cos\theta_6 + \sin\theta_6\sin\theta_4\cos(\phi_6-\phi_4) \\ &+ \cos\theta_6\cos\theta_4\big] + \frac{1}{3}j\big[\sin\theta_1\sin\theta_4\cos(\phi_1-\phi_4) + \cos\theta_1\cos\theta_4 \\ &+ \sin\theta_2\sin\theta_5\cos(\phi_2-\phi_5) + \cos\theta_2\cos\theta_5 + \sin\theta_3\sin\theta_6\cos(\phi_3-\phi_6) \\ &+ \cos\theta_3\cos\theta_6\big] - \frac{1}{2}h\big(\sin\theta_1\cos\phi_1 + \sin\theta_2\cos\phi_2 + \sin\theta_3\cos\phi_3 \\ &+ \sin\theta_4\cos\phi_4 + \sin\theta_5\cos\phi_5 + \sin\theta_6\cos\phi_6\big) \\ &+ \frac{1}{6}d\big(\cos^2\theta_1 + \cos^2\theta_2 + \cos^2\theta_3 + \cos^2\theta_4 + \cos^2\theta_5 + \cos^2\theta_6\big) \end{aligned} \tag{2.2}$$

where $j = J_{\parallel}/J_{\perp}$, $h = g\mu_B H/6J_{\perp}S$ and $d = D/2J_{\perp}$. Minimization of e_0 with respect to the twelve variables θ_s, ϕ_s is performed numerically. We are interested in the limit $j \ll 1$, suitable for BX_2 compounds. The opposite limit $j \gg 1$, suitable for ABX_3 compounds, was studied in [10] where a single-ion easy-plane anisotropy was chosen. The minimum-energy configurations that we find are two umbrella (U1, U2) and two planar (P, SF) spin configurations as shown in figure 2. The umbrella configurations are stable for small single-ion anisotropy.

The U1 configuration corresponds to a phase with θ_1, θ_2, $\theta_3 = \theta_2$, $\theta_4 = \pi - \theta_1$, $\theta_5 = \theta_6 = \pi - \theta_2$, $\phi_1 = \phi_4 = 0$, ϕ_2, $\phi_3 = \phi_5 = -\phi_2$, $\phi_6 = \phi_2$, where θ_1, θ_2, ϕ_2 are

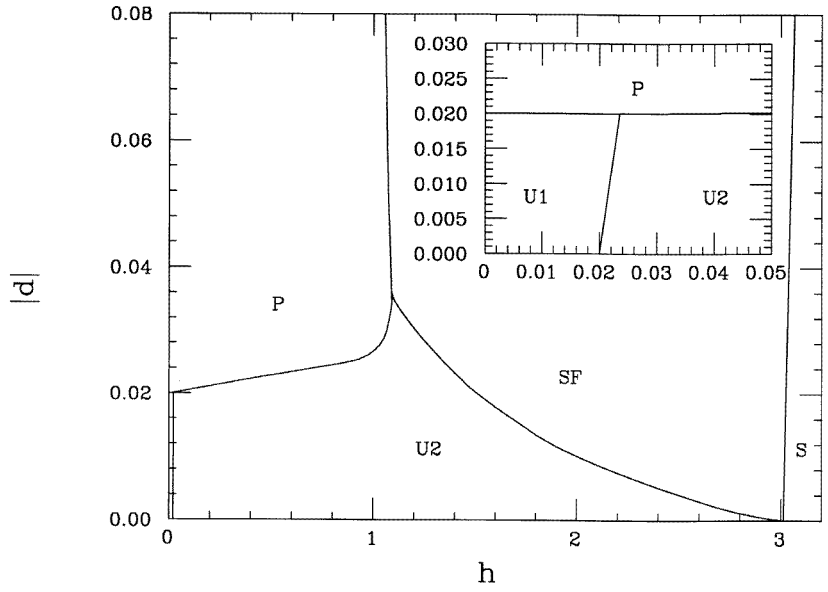

Figure 2. The zero-temperature phase diagram in the $h, |d|$ plane for $j = 0.01$. U1, U2, P, SF, and S mean the umbrellas of two kinds discussed in section 2, planar, spin-flop like, and saturated phase. The inset illustrates the physical region of the phase diagram.

solutions of the equations

$$\begin{aligned}
&\sin\theta_2 \sin\phi_2 \left[-\left(1+\frac{2}{3}j\right)\sin\theta_2\cos\phi_2 - \frac{1}{2}\sin\theta_1 + \frac{1}{2}h \right] = 0 \\
&\cos\theta_1 \left[\sin\theta_2\cos\phi_2 + \left(\frac{2}{3}j - \frac{1}{3}d\right)\sin\theta_1 - \frac{1}{2}h \right] = \sin\theta_1\cos\theta_2 \\
&\cos\theta_2 \left[-\sin\theta_2\sin^2\phi_2 + \frac{1}{2}\sin\theta_1\cos\phi_2 + \frac{2}{3}j\sin\theta_2\cos^2\phi_2 \right. \\
&\qquad \left. -\frac{1}{2}h\cos\phi_2 - \frac{1}{3}d\sin\theta_2 \right] \\
&\qquad = \frac{1}{2}\cos\theta_1\sin\theta_2.
\end{aligned} \tag{2.3}$$

For small h and d we obtain

$$\begin{aligned}
\cos\phi_2 &\simeq \frac{(1+d/3)[4j/3 - d + 2d(2j-d)/9]}{2(2j-d)\sqrt{3/4 + 2d/3 + d^2/9}[1 + 2(2j+d)/9 + 4dj/27]}h \\
\sin\theta_1 &\simeq \frac{(1+d/3)2j/3}{(2j-d)[1+2(2j+d)/9+4dj/27]}h \\
\cos\theta_2 &= \frac{-1/2}{1+d/3} + \mathrm{O}(h^2)
\end{aligned} \tag{2.4}$$

and

$$e_0^{(\mathrm{U1})} \simeq \frac{-3/2 + d^2/9}{1+d/3} - j - \frac{1}{2}h^2 + \frac{1}{9}jh^2\frac{4j-3d}{2j-d}. \tag{2.5}$$

The U2 phase is characterized by $\theta_1 = \theta_4 = \pi/2$, θ_2, $\theta_3 = \theta_5 = \pi - \theta_2$, $\theta_6 = \theta_2$, ϕ_1, ϕ_2, $\phi_3 = \phi_2$, $\phi_4 = -\phi_1$, $\phi_5 = \phi_6 = -\phi_2$, where ϕ_1, ϕ_2, θ_2 are solutions of the equations

$$\begin{aligned}
&-\sin\theta_2 \sin(\phi_1 - \phi_2) - \frac{1}{3} j \sin 2\phi_1 + \frac{1}{2} h \sin\phi_1 = 0 \\
&\sin\theta_2 \left[\frac{1}{2} \sin(\phi_1 - \phi_2) - \frac{1}{3} j \sin\theta_2 \sin 2\phi_2 + \frac{1}{2} h \sin\phi_2 \right] = 0 \\
&\cos\theta_2 \left[\frac{1}{2} \cos(\phi_1 - \phi_2) + \sin\theta_2 + \frac{2}{3} j \sin\theta_2 \cos^2\phi_2 - \frac{1}{2} h \cos\phi_2 - \frac{1}{3} d \sin\theta_2 \right] = 0.
\end{aligned} \tag{2.6}$$

For small h and d we obtain

$$\begin{aligned}
\cos\phi_1 &\simeq \frac{(2j - d)(1 - d/3)}{2j[1 + 2(1 - d/3)^2 + 4(1 - d/3) j/3]} h \\
\cos\phi_2 &\simeq \frac{(1 - d/3)[d + 4j(1 - d/3)]}{2j[1 + 2(1 - d/3)^2 + 4(1 - d/3) j/3]} h \\
\sin\theta_2 &= \frac{1/2}{1 - d/3} + \mathrm{O}(h^2)
\end{aligned} \tag{2.7}$$

and

$$e_0^{(\mathrm{U2})} \simeq \frac{-3/2 + 3d/2 - 5d^2/9 + 2d^3/27}{(1 - d/3)^2} - j - \frac{1}{2} h^2 + \frac{2}{9} j h^2 \left(1 + \frac{d}{4j} \right) \left(1 - \frac{d}{2j} \right). \tag{2.8}$$

Note that both U1 and U2 phases have been found in ABX_3 compounds [10, 11].

The P phase is characterized by θ_1, θ_2, θ_3, $\theta_4 = \pi - \theta_1$, $\theta_5 = \pi - \theta_3$, $\theta_6 = \pi - \theta_2$, $\phi_1 = \phi_2 = \phi_4 = \phi_6 = 0$, $\phi_3 = \phi_5 = \pi$, where θ_1, θ_2, θ_3 are solutions of the equations

$$\begin{aligned}
&\cos\theta_1 \left[\sin\theta_2 - \sin\theta_3 + \left(\frac{4}{3} j - \frac{2}{3} d \right) \sin\theta_1 - h \right] = \sin\theta_1 (\cos\theta_2 + \cos\theta_3) \\
&\cos\theta_2 \left(\sin\theta_1 - \sin\theta_3 - \frac{2}{3} j \sin\theta_3 - h - \frac{2}{3} d \sin\theta_2 \right) \\
&\qquad = \sin\theta_2 \left[\cos\theta_1 + \left(1 - \frac{2}{3} j \right) \cos\theta_3 \right] \\
&-\cos\theta_3 \left(\sin\theta_1 + \sin\theta_2 + \frac{2}{3} j \sin\theta_2 - h + \frac{2}{3} d \sin\theta_3 \right) \\
&\qquad = \sin\theta_3 \left[\cos\theta_1 + \left(1 - \frac{2}{3} j \right) \cos\theta_2 \right].
\end{aligned} \tag{2.9}$$

For small h and d we obtain

$$\begin{aligned}
\sin\theta_1 &\simeq \frac{2 - 8(2j + d)(1 + d/3)^2/3 - 2(1 - d/3)}{2 - [8(2j + d)(1 + d/3)^2/3 + 2(1 - d/3)][4j/3 - 2d/3 + (1 + d/3)^{-1}]} h \\
\sin\theta_2 &\simeq \sqrt{1 - [2(1 + d/3)]^{-2}} \\
&\qquad + \frac{1 - [4j/3 - 2d/3 + (1 + d/3)^{-1}]}{2 - [8(2j + d)(1 + d/3)^2/3 + 2(1 - d/3)][4j/3 - 2d/3 + (1 + d/3)^{-1}]} h \\
\sin\theta_3 &\simeq \sqrt{1 - [2(1 + d/3)]^{-2}} \\
&\qquad - \frac{1 - [4j/3 - 2d/3 + (1 + d/3)^{-1}]}{2 - [8(2j + d)(1 + d/3)^2/3 + 2(1 - d/3)][4j/3 - 2d/3 + (1 + d/3)^{-1}]} h
\end{aligned} \tag{2.10}$$

and

$$e_0^{(\mathrm{P})} \simeq \frac{-3/2 + d^2/9}{1 + d/3} - j - \frac{1}{2}h^2 + \frac{4}{9}jh^2\left(1 - \frac{3d}{4j}\right)\left(1 + \frac{3d}{8j}\right). \tag{2.11}$$

The planar spin-flop-like SF phase is characterized by $\phi_s = 0$ for $s = 1, \ldots, 6$, $\theta_1 = \theta_4 = \pi/2$, $\theta_3 = \theta_5 = \pi - \theta_2$, $\theta_6 = \theta_2$ with

$$\theta_2 = \sin^{-1}\frac{(h-1)/2}{1 + 2j/3 - d/3} \tag{2.12}$$

$$e_0^{(\mathrm{SF})} = -1 - j/3 + 2d/3 - h - \frac{(h-1)^2}{2(1 + 2j/3 - d/3)}. \tag{2.13}$$

The saturated (S) phase corresponds to $\phi_s = 0$, $\theta_s = \pi/2$ for $s = 1, \ldots, 6$, $e_0^{(\mathrm{S})} = 3 + j - 3h$. The S phase is stable for $h > h_s = 3 + 2(2j - d)/3$.

In figure 2 we show the zero-temperature phase diagram for the model (2.1) in the $h, |d|$ plane for $j = 0.01$, a typical value of exchange coupling for BX_2 compounds [2]. Note that the actual magnetic fields are restricted to the region of small h, say $h < 0.1$; indeed $h = 0.1$ corresponds to $H = 10$ T for $J_\perp$ of the order of 20 K [2]. In this region of low magnetic field only U1, U2, and P phases are found, as shown by the inset of figure 2. The classical phase boundaries obtained by comparing the energies of the various phases are listed below.

(i) The U1–P phase boundary is

$$|d| = 2j.$$

(ii) The U1–U2 phase boundary is

$$h \simeq 2\sqrt{j(2j - d)/3}.$$

(iii) The U2–P phase boundary is

$$h \simeq |d|\sqrt{|d|/[6j(1 + |d|/2j - 7d^2/16j^2)]}.$$

(All of these phase transitions are first order—as is the P–SF one which occurs at $h \simeq 1.1$. The remaining two phase transitions are second order.)

(iv) The U2–SF phase boundary is

$$h = 1 + \frac{2(1 + 2j/3 - d/3)(1 + d/4j - d/3)}{(1 - d/3)(1 - d/2j)}.$$

(v) The SF–S phase boundary is

$$h = 3 + 2(2j + |d|)/3.$$

Note that the parameters suitable for VBr_2 [2] ($j = 0.01$, $d = -0.003$, $0 < h < 0.015$) imply that the stable phase is the U1 phase. A transition to the U2 phase should be expected at a field of the order of 2 T. However, this classical scenario is dramatically changed by quantum fluctuations as we will show in section 4.

For the isotropic Heisenberg hexagonal antiferromagnet ($d = 0$) one has that the two phases U1 and U2 reduce to a regular umbrella phase where the spins are spiralling on the surface of a cone with its axis along the field direction, apex angle $\theta = \cos^{-1}((3h/(9 + 4j))$, and energy $e_0^{(\mathrm{U})} = -\frac{3}{2} - j - 9h^2(2(9 + 4j))$. The P and SF phases reduce to the phases 7 and 5C of [12], respectively. For vanishing magnetic field the energy of the P phase is $e_0^{(\mathrm{P})} = -\frac{3}{2} - j - 9h^2/(2(9 + 8j))$. Note that the planar model studied in [12] does not have a quantum counterpart, so the effect of quantum fluctuations—that is the target of the present

Table 1. Comparison of the classical energies of the U ($e_0^{(U)}$), P ($e_0^{(P)}$) and SF phases ($e_0^{(SF)}$) as functions of the external magnetic field for $j = 0.01$.

h	$e_0^{(U)}$	$e_0^{(P)}$	$e_0^{(SF)}$
0	−1.510 000	−1.510 000	
0.1	−1.514 978	−1.514 956	
0.2	−1.529 912	−1.529 823	
0.3	−1.554 801	−1.554 600	
0.4	−1.589 646	−1.589 282	
0.5	−1.634 447	−1.633 867	
0.6	−1.689 204	−1.688 345	
0.7	−1.753 916	−1.752 708	
0.8	−1.828 584	−1.826 944	
0.9	−1.913 208	−1.911 050	
1.0	−2.007 788	−2.005 066	−2.003 333
1.1	−2.112 323	−2.109 098	−2.108 300
1.2	−2.226 814	−2.223 228	−2.223 201
1.3	−2.351 261	−2.347 475	−2.348 035
1.4	−2.485 664	−2.481 832	−2.482 804
1.5	−2.630 022	−2.626 283	−2.627 506
1.6	−2.784 336	−2.780 814	−2.782 141
1.7	−2.948 606	−2.946 711	−2.945 411
1.8	−3.122 832	−3.120 062	−3.121 214
1.9	−3.307 013	−3.304 759	−3.305 651
2.0	−3.501 150	−3.499 393	−3.500 022
2.5	−4.621 173	−4.620 822	−4.649 670
2.6	−4.875 044	−4.874 826	−4.874 857
2.7	−5.138 872	−5.138 751	−5.138 764
2.8	−5.412 655	−5.412 601	−5.412 605
2.9	−5.696 394	−5.696 379	−5.696 380
3.0	−5.990 0885	−5.990 0883	−5.990 0883
3.013 33	−6.030 000	−6.030 000	−6.030 000

work—is beyond that model. Moreover, the planar phases 7, 5C are at most metastable phases for the isotropic classical Heisenberg model for which the absolute minimum of energy is achieved by the umbrella phase.

As one can see from table 1, where the classical energies of the U, P and SF phases of the isotropic model with $j = 0.01$ are compared for different magnetic fields, the U phase is stable with respect to the P phase for any magnetic field. Obviously the U and P phases coincide at $h = 0$ and at the saturation field $h = h_s = 3.013\,33$. The P phase coincides with the phase 7 of [12] for $h < 1.895$. At $h = 1.895$ the phase 7 becomes the phase 5A of [12]. The phase 5C (SF) is stable with respect to the phase 7 (P) for $h > 1.203$. In any case the absolute minimum corresponds to the U phase.

3. Magnon frequencies

In order to find the spin-wave frequencies a generalization of the customary approach is used. Six transformations from the crystal axis to the local axis are introduced:

$$\begin{pmatrix} S_{i,x}^{(s)} \\ S_{i,y}^{(s)} \\ S_{i,z}^{(s)} \end{pmatrix} = \begin{pmatrix} \cos\theta_s \cos\phi_s & -\sin\phi_s & \sin\theta_s \cos\phi_s \\ \cos\theta_s \sin\phi_s & \cos\phi_s & \sin\theta_s \sin\phi_s \\ -\sin\theta_s & 0 & \cos\theta_s \end{pmatrix} \begin{pmatrix} S_{i,\xi}^{(s)} \\ S_{i,\eta}^{(s)} \\ S_{i,\zeta}^{(s)} \end{pmatrix} \tag{3.1}$$

with $s = 1, \ldots, 6$ running over the six sublattices of the HAF model. Then the harmonic boson equivalent Hamiltonian is obtained by the linearized spin-boson transformation:

$$\begin{aligned} S_{i,\xi}^{(s)} &\simeq \sqrt{2S}(a_i^{(s)} + a_i^{(s)\dagger})/2 \\ S_{i,\eta}^{(s)} &\simeq \sqrt{2S}(a_i^{(s)\dagger} - a_i^{(s)})/2\mathrm{i} \\ S_{i,\zeta}^{(s)} &= S - a_i^{(s)\dagger} a_i^{(s)}. \end{aligned} \tag{3.2}$$

Finally the spatial Fourier transform of the localized spin deviation operators is performed:

$$a_i^{(s)} = \sqrt{6/N} \sum_{\boldsymbol{k}} \mathrm{e}^{\mathrm{i}\boldsymbol{k}\cdot\boldsymbol{r}_i} a_{\boldsymbol{k}}^{(s)}. \tag{3.3}$$

Substitution of (3.1)–(3.3) in Hamiltonian (2.1) gives

$$\begin{aligned} \mathcal{H} = E_0(\theta_s, \phi_s) &+ \frac{1}{6} DSN \sum_{s=1}^{6} \cos^2\theta_s - \frac{1}{12} g\mu_B HN \sum_{s=1}^{6} \cos\theta_s \sin\theta_s \\ &+ J_\perp SN\big(r_{12} + r_{23} + r_{31} + r_{45} + r_{56} + r_{64}\big) + \frac{2}{3} J_\parallel SN\big(r_{14} + r_{25} + r_{36}\big) \\ &+ \sum_{\boldsymbol{k}} \big(\mathbf{A}_{\boldsymbol{k}}^\dagger, \mathbf{A}_{-\boldsymbol{k}}\big) \begin{pmatrix} \mathbf{H}(\boldsymbol{k}) & \mathbf{M}^*(-\boldsymbol{k}) \\ \mathbf{M}(\boldsymbol{k}) & \mathbf{H}^*(-\boldsymbol{k}) \end{pmatrix} \begin{pmatrix} \mathbf{A}_{\boldsymbol{k}} \\ \mathbf{A}_{-\boldsymbol{k}}^\dagger \end{pmatrix} \end{aligned} \tag{3.4}$$

where $E_0(\theta_s, \phi_s)$ is given by (2.2), and the column matrix of boson operators $\mathbf{A}_{\boldsymbol{k}}$ and the matrix elements of $\mathbf{H}(\boldsymbol{k})$ and $\mathbf{M}(\boldsymbol{k})$ in (3.4) are given in appendix A. The $r_{ss'}$ are given by (A.36).

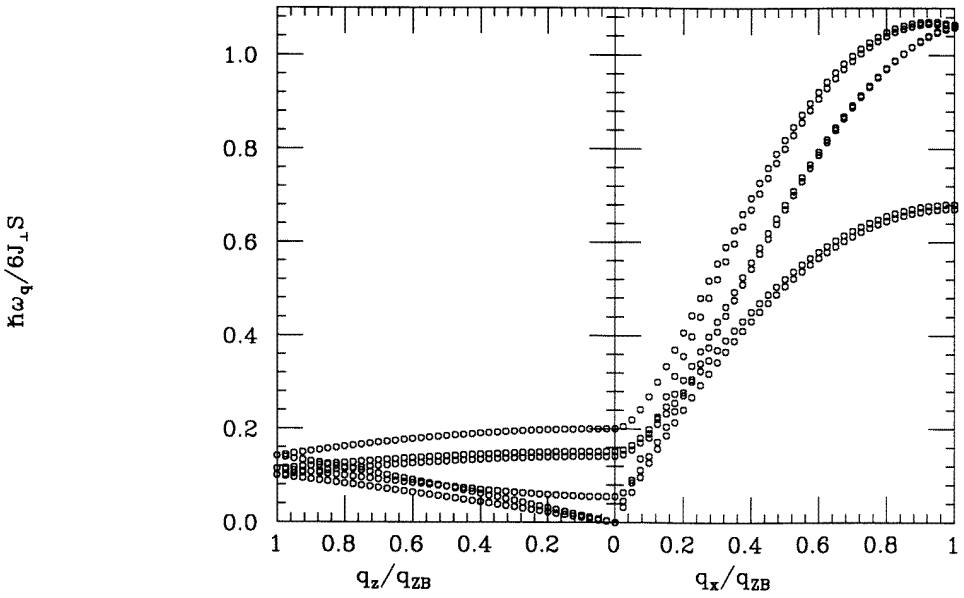

Figure 3. Magnon frequencies for the U1 phase along q_z (0,0,ζ) and q_x (ξ, ξ, 0) for $h = 0$.

Introducing the following Bogoliubov transformation:

$$\alpha_{\boldsymbol{k}}^{(s)} = \sum_{r=1}^{6} \big(u_{\boldsymbol{k}}^{(s,r)} a_{\boldsymbol{k}}^{(r)} - v_{\boldsymbol{k}}^{(s,r)} a_{-\boldsymbol{k}}^{(r)\dagger}\big) \tag{3.5}$$

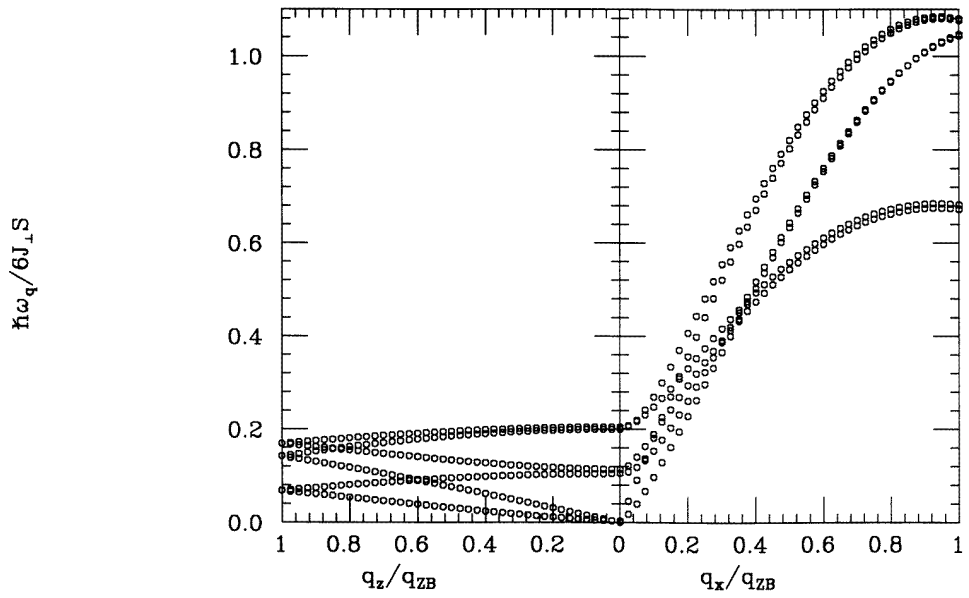

Figure 4. Magnon frequencies for the U2 phase along q_z (0,0,ζ) and q_x (ξ, ξ, 0) for $h = 0.1$.

with $s = 1, \ldots, 6$, Hamiltonian (3.4) becomes

$$\mathcal{H} = E_0(\theta_s, \phi_s) + \frac{1}{6}DSN\sum_{s=1}^{6}\cos^2\theta_s - \frac{1}{12}g\mu_B HN\sum_{s=1}^{6}\cos\theta_s \sin\theta_s$$
$$+J_\perp SN\left(r_{12}+r_{23}+r_{31}+r_{45}+r_{56}+r_{64}\right)+\frac{2}{3}J_\parallel SN\left(r_{14}+r_{25}+r_{36}\right)$$
$$+\sum_{\boldsymbol{k}}\sum_{s=1}^{6}\frac{1}{2}\overline{h}\omega_{\boldsymbol{k}}^{(s)}+\sum_{\boldsymbol{k}}\sum_{s=1}^{6}\overline{h}\omega_{\boldsymbol{k}}^{(s)}\alpha_{\boldsymbol{k}}^{(s)\dagger}\alpha_{\boldsymbol{k}}^{(s)} \tag{3.6}$$

where $\overline{h}\omega_{\boldsymbol{k}}^{(s)}$ are solutions of the following determinantal equation obtained via the equation of motion for the $\alpha_{\boldsymbol{k}}^{(s)}$-operators:

$$\det\begin{pmatrix}\mathbf{H}^*(\boldsymbol{k})-\frac{1}{2}\overline{h}\omega_{\boldsymbol{k}}^{(s)}\mathbf{1} & \mathbf{M}(-\boldsymbol{k})\\ -\mathbf{M}^*(\boldsymbol{k}) & -\mathbf{H}(-\boldsymbol{k})-\frac{1}{2}\overline{h}\omega_{\boldsymbol{k}}^{(s)}\mathbf{1}\end{pmatrix}=0. \tag{3.7}$$

Note that in (3.6) the first term is the classical energy, the next five terms are the zero-point-motion energy and the last one is the harmonic Hamiltonian diagonal in the new boson operators. In figures 3 and 4 we give the spin-wave dispersion relations for $j = 0.01$, $d = -0.003$, $h = 0$ and $h = 0.1$, respectively. The uniform modes are expected at 0, 0.0017, 0.683, 1.752, 1.882, 2.481 meV for $h = 0$, and at 0.0093, 0.043, 1.298, 1.414, 2.479, 2.539 meV for $h = 0.1$ (corresponding to $H = 10$ T), respectively.

4. Zero-point-motion energy of the isotropic model

Owing to the small value of the single-ion anisotropy [2] we can evaluate the zero-point-motion energy in the isotropic limit ($d = 0$). In this case we obtain much simpler expressions

for the U phase where the spins are regularly spiralling on the surface of a cone, so the standard approach for treating regular helices can be applied. Transformation (3.1) can be used changing ϕ_s into $\boldsymbol{Q}\cdot\boldsymbol{r}_i$ and θ_s into the apex angle of the cone θ. In this way we have only one kind of operator instead of six and we obtain

$$\mathcal{H} = E_0(\theta,\boldsymbol{Q}) + \sum_{\boldsymbol{k}} A_{\boldsymbol{k}} a_{\boldsymbol{k}}^{\dagger} a_{\boldsymbol{k}} + \frac{1}{2}\sum_{\boldsymbol{k}} B_{\boldsymbol{k}}\left(a_{\boldsymbol{k}} a_{-\boldsymbol{k}} + a_{\boldsymbol{k}}^{\dagger} a_{-\boldsymbol{k}}^{\dagger}\right) \tag{4.1}$$

where

$$E_0(\theta,\boldsymbol{Q}) = -\sum_{\boldsymbol{\delta}_\perp} J_\perp S^2 N\left(\sin^2\theta\cos\boldsymbol{Q}\cdot\boldsymbol{\delta}_\perp + \cos^2\theta\right) - \sum_{\boldsymbol{\delta}_\parallel} J_\parallel S^2 N\left(\sin^2\theta\cos\boldsymbol{Q}\cdot\boldsymbol{\delta}_\parallel + \cos^2\theta\right) - g\mu_B H S N\cos\theta \tag{4.2}$$

$$A_{\boldsymbol{k}} = A_{\boldsymbol{k}}^{(1)}(\theta,\boldsymbol{Q}) + A_{\boldsymbol{k}}^{(2)}(\theta,\boldsymbol{Q}) \tag{4.3}$$

with

$$A_{\boldsymbol{k}}^{(1)}(\theta,\boldsymbol{Q}) = -2S\Big\{\cos^2\theta\big[J(0) - J(\boldsymbol{Q})\big] + J(\boldsymbol{Q}) - \tfrac{1}{2}\big[J(\boldsymbol{k}+\boldsymbol{Q}) + J(\boldsymbol{k}-\boldsymbol{Q})\big] - \tfrac{1}{2}\sin^2\theta\big[J(\boldsymbol{k}) - \tfrac{1}{2}(J(\boldsymbol{k}+\boldsymbol{Q}) + J(\boldsymbol{k}-\boldsymbol{Q}))\big]\Big\} + g\mu_B H\cos\theta \tag{4.4}$$

$$A_{\boldsymbol{k}}^{(2)}(\theta,\boldsymbol{Q}) = -S\cos\theta\big[J(\boldsymbol{k}-\boldsymbol{Q}) - J(\boldsymbol{k}+\boldsymbol{Q})\big] \tag{4.5}$$

$$B_{\boldsymbol{k}} = S\sin^2\theta\big[J(\boldsymbol{k}) - \tfrac{1}{2}(J(\boldsymbol{k}+\boldsymbol{Q}) + J(\boldsymbol{k}-\boldsymbol{Q}))\big] \tag{4.6}$$

$$J(\boldsymbol{Q}) = 2J_\perp\big[\cos(aQ_x) + 2\cos(aQ_x/2)\cos(\sqrt{3}aQ_y/2) + j\cos(cQ_z)\big]. \tag{4.7}$$

Minimization with respect to θ and $\boldsymbol{Q}$ gives the apex angle

$$\theta = \cos^{-1}\frac{g\mu_B H}{2S[J(\boldsymbol{Q}) - J(0)]}$$

and the helix wave vector $\boldsymbol{Q} = (4\pi/(3a), 0, \pi/c)$. The usual Bogoliubov transformation can be used to give

$$\mathcal{H} = E_0 + \Delta E + \sum_{\boldsymbol{k}} \hbar\omega_{\boldsymbol{k}}\alpha_{\boldsymbol{k}}^{\dagger}\alpha_{\boldsymbol{k}} \tag{4.8}$$

where

$$\Delta E = -\tfrac{1}{2}\sum_{\boldsymbol{k}} A_{\boldsymbol{k}}^{(1)} + \tfrac{1}{2}\sum_{\boldsymbol{k}}\sqrt{A_{\boldsymbol{k}}^{(1)2} - B_{\boldsymbol{k}}^2} \tag{4.9}$$

is the zero-point-motion energy. The magnon energy is

$$\hbar\omega_{\boldsymbol{k}} = \sqrt{A_{\boldsymbol{k}}^{(1)2} - B_{\boldsymbol{k}}^2} + A_{\boldsymbol{k}}^{(2)}. \tag{4.10}$$

Note that $\hbar\omega_{\boldsymbol{k}}$ is different from $\hbar\omega_{-\boldsymbol{k}}$. The reduced ground-state energy

$$e_G^{(\mathrm{U})} = (E_0 + \Delta E)/(2J_\perp N S^2)$$

is given by

$$e_G^{(\mathrm{U})} = -\frac{3}{2} - \frac{h^2}{2}\frac{1}{1+4j/9} - j - \frac{1}{S}\left(\frac{3}{2} + j\right) + \frac{1}{2S}\Delta^{(\mathrm{U})}(h,j) \tag{4.11}$$

where

$$\Delta^{(\mathrm{U})}(h,j) = \frac{1}{\pi^3}\int_0^\pi \mathrm{d}x\int_0^\pi \mathrm{d}y\int_0^\pi \mathrm{d}z\,\sqrt{s(x,y,z)d(x,y,z)} \tag{4.12}$$

with

$$s(x,y,z) = 3 + 2\cos(2x) + 4\cos x\cos y + 2j(1+\cos z) - \frac{9h^2}{(9+4j)^2}[3\cos(2x) + 6\cos x\cos y + 4j\cos z] \tag{4.13}$$

$$d(x,y,z) = 3 - \cos(2x) - 2\cos x\cos y + 2j(1-\cos z). \tag{4.14}$$

In the limit of vanishing j the reduced ground-state energy is

$$e_G^{(\mathrm{U})}(j\to 0) = -\frac{3}{2} - \frac{1}{2}h^2 - j\left(1 - \frac{2}{9}h^2\right) - \frac{3}{2S} + \frac{1}{2S}\Delta^{(\mathrm{U})}(h,0). \tag{4.15}$$

This expansion is justified by the small value of j suitable for BX_2 compounds [2] and it is useful in view of the comparison we will make with a similar expansion for the planar configuration.

The planar phase P does not correspond to a regular helix, so the formulae of section 3 should have been used. However, the P configuration for vanishing anisotropy corresponds to a secondary minimum of the classical energy, since the absolute minimum corresponds to a U configuration. For this reason the elementary excitation energies are not well defined. Indeed we have found imaginary frequencies in a narrow region around the centre of the Brillouin zone. We stress that this drawback is not peculiar to the model that we consider but is common for all isotropic Heisenberg models since the elementary excitation energies are well defined only for the absolute minimum of the classical energy. This limitation is obviously unphysical and it is related to the customary expansion in $1/S$. We overcome this problem by taking advantage of the smallness of the interlayer coupling. In this limit we may consider the HAF model as a stacking of TAF layers in each of which the elementary excitations are well defined in an infinity of inequivalent configurations that are isoenergetic in the classical approximation [7]. It is well known that the zero-point motion selects a single configuration where, for small h, one spin over three is antiparallel to the field. On the other hand the energy contribution from the interlayer coupling that we take into account in the classical approximation is minimized by a configuration where a spin in a layer makes an angle ϕ with the external magnetic field and its NN spins in the adjacent layers make an angle $-\phi$ with respect to the field. The reduced classical energy reads

$$e_0^{(\mathrm{P})} = -\frac{3}{2} - \frac{1}{2}h^2 + je_0(h,\phi) \tag{4.16}$$

where

$$e_0(h,\phi) = \frac{1}{3}\left(2\cos^2\phi + 1 - \frac{4\sin^2\phi}{1+h^2-2h\cos\phi}\right). \tag{4.17}$$

The value of ϕ is arbitrary owing to the degeneracy of the classical minimum-energy configuration of the TAF model [6]. The spin configuration for the six sublattices of the HAF model is

$$\phi_1 = \phi$$

$$\cos\phi_2 = \frac{1}{2}\left(h - \cos\phi - \sin\phi\sqrt{\frac{3-h^2+2h\cos\phi}{1+h^2-2h\cos\phi}}\right)$$
$$\sin\phi_2 = -\frac{1}{2}\left[\sin\phi + (h-\cos\phi)\sqrt{\frac{3-h^2+2h\cos\phi}{1+h^2-2h\cos\phi}}\right]$$
$$\cos\phi_3 = \frac{1}{2}\left(h - \cos\phi + \sin\phi\sqrt{\frac{3-h^2+2h\cos\phi}{1+h^2-2h\cos\phi}}\right) \tag{4.18}$$
$$\sin\phi_2 = -\frac{1}{2}\left[\sin\phi - (h-\cos\phi)\sqrt{\frac{3-h^2+2h\cos\phi}{1+h^2-2h\cos\phi}}\right]$$
$$\phi_4 = -\phi \qquad \phi_5 = -\phi_3 \qquad \phi_6 = -\phi_2.$$

Note that in the absence of anisotropy the spins lie in an arbitrary plane containing the magnetic field. The reduced ground-state energy reads

$$e_G^{(\mathrm{P})} = e_0^{(\mathrm{P})} - \frac{3}{2S} + \frac{1}{2S}\,\Delta^{(\mathrm{P})}(h,\phi) \tag{4.19}$$

where [13]

$$\Delta^{(\mathrm{P})}(h,\phi) = \frac{1}{\pi^2}\int_0^\pi \mathrm{d}x \int_0^\pi \mathrm{d}y \sum_{s=1}^{3}\sqrt{\lambda^{(s)}(x,y)}. \tag{4.20}$$

The $\lambda^{(s)}$ with $s = 1, 2, 3$ are the roots of the equation

$$\lambda^3 - \left(3+2s_1|\gamma|^2\right)\lambda^2 + \left[3-(3+s_2-s_1)|\gamma|^2 + s_1^2|\gamma|^4 - (s_1^2 - s_2 + 2s_1)\left(\gamma^3+\gamma^{*3}\right)/2\right]\lambda$$
$$-\left[1-s_2|\gamma|^2 + (s_2-1)\left(\gamma^3+\gamma^{*3}\right)/2\right]\left[1-3|\gamma|^2+\gamma^3+\gamma^{*3}\right]$$
$$= 0 \tag{4.21}$$

with

$$\gamma = \frac{1}{3}\left(\mathrm{e}^{\frac{2}{3}\mathrm{i}x} + 2\mathrm{e}^{-\frac{1}{3}\mathrm{i}x}\cos y\right) \tag{4.22}$$

$$s_1 = -\frac{3}{2} + \frac{1}{2}h^2 \qquad s_2 = \frac{1}{4}\left[3 + h^2\rho(h,\phi)\right] \tag{4.23}$$

$$\rho(h,\phi) = \frac{4 - 4h\cos\phi(4\cos^2\phi - 1) + h^2(16\cos^2\phi - 3) - 6h^3\cos\phi + h^4}{1 - 2h\cos\phi + h^2} \tag{4.24}$$

where $0 < \phi < \pi$ for $0 < h < 1$ and $0 < \phi < \phi_M = \cos^{-1}((h^2-3)/2h)$ for $1 < h < 3$. Note that $e_0^{(\mathrm{P})}$ is minimum for $\phi = \phi_m$ given by the real solution of the equation

$$4h^2\cos^3\phi_m - 2h(3+2h^2)\cos^2\phi_m + (3+4h^2+h^4)\cos\phi_m - 2h = 0. \tag{4.25}$$

In the limit of small h one has

$$\cos\phi_m = \frac{2}{3}h - \frac{2}{81}h^5 + \cdots. \tag{4.26}$$

In contrast $\Delta^{(\mathrm{P})}(h,\phi)$ is minimized by

$$\phi = \phi_0 = \cos^{-1}\left(\frac{1+h}{2}\right) \qquad \text{and} \qquad \phi = \pi$$

for $0 < h < 1$ and by

$$\phi = \phi_0 = \cos^{-1}\left(\frac{h^2+3}{4h}\right) \qquad \text{and} \qquad \phi = \phi_M$$

for $1 < h < 3$. Note that the configurations corresponding to the two minima of $\Delta^{(\mathrm{P})}(h,\phi)$ are equivalent in the 2D TAF model but not equivalent in the 3D HAF model, where they lead to a different interlayer energy contribution $e_0(h,\phi)$.

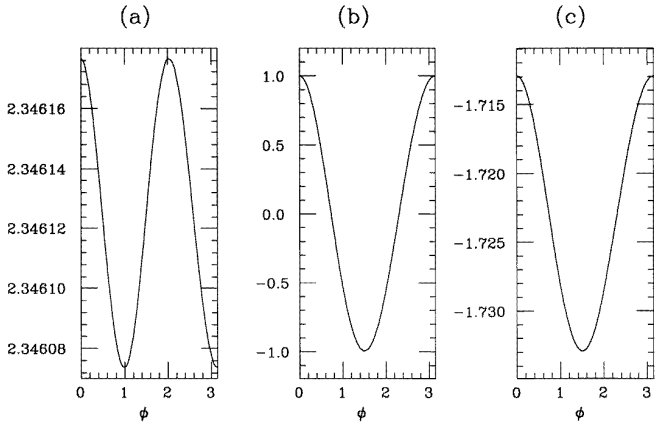

Figure 5. (a) $\Delta^{(\mathrm{P})}(h = 0.1, \phi)$ given by equation (4.20), (b) $e_0(h = 0.1, \phi)$ given by equation (4.17), and (c) $e_G^{(\mathrm{P})}$ given by equation (4.19) for $S = 3/2$, $j = 0.01$.

In figure 5 we show: (a) $\Delta^{(\mathrm{P})}(h,\phi)$ given by equation (4.20); (b) $e_0(h,\phi)$ given by equation (4.17); and (c) $e_G^{(\mathrm{P})}$ given by equation (4.19) for $j = 0.01$, $S = 3/2$ and $h = 0.1$ as functions of ϕ. As one can see, the value $\phi = 1.5029$ at which $e_G^{(\mathrm{P})}$ is a minimum is very close to $\phi_m = 1.5041$ at which $e_0(0.1,\phi)$ is a minimum. Note that the minima of $\Delta^{(\mathrm{P})}(0.1,\phi)$ occur at $\phi = \phi_0 = 0.9884$ and $\phi = \pi$.

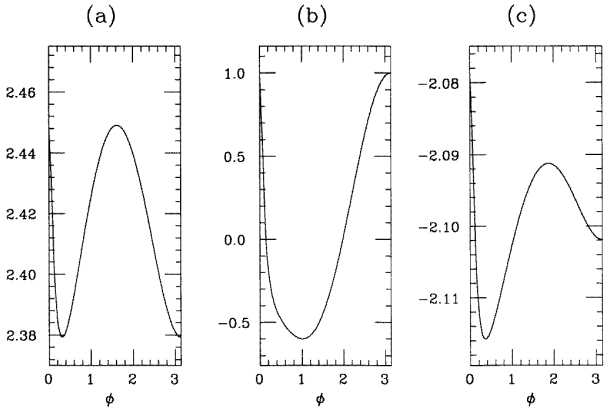

Figure 6. (a) $\Delta^{(\mathrm{P})}(h = 0.9, \phi)$, (b) $e_0(h = 0.9, \phi)$, and (c) $e_G^{(\mathrm{P})}$ for $S = 3/2$, $j = 0.01$.

In figure 6 we show the same quantities for $h = 0.9$. The minima of $\Delta^{(\mathrm{P})}(0.9,\phi)$ occur at $\phi = \phi_0 = 0.3176$ and $\phi = \pi$. The minima of $e_0(0.9,\phi)$ and $e_G^{(\mathrm{P})}$ occur at

$\phi = \phi_m = 1.0141$ and $\phi = 0.3604$, respectively. The zero-point-motion energy becomes crucial in selecting the spin configuration.

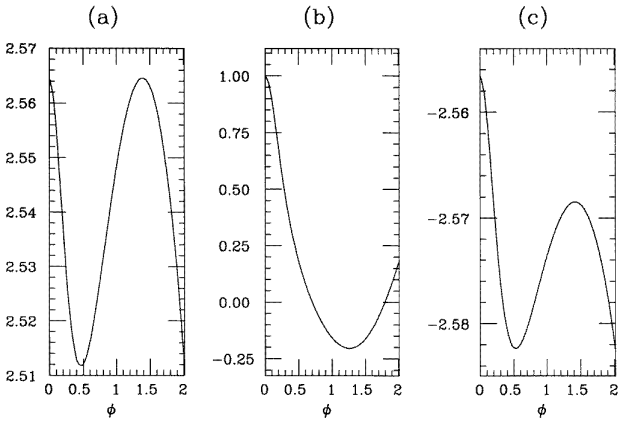

Figure 7. (a) $\Delta^{(P)}(h = 1.357\,53, \phi)$, (b) $e_0(h = 1.357\,53, \phi)$, and (c) $e_G^{(P)}$ for $S = 3/2$, $j = 0.01$.

In figure 7 we show a first-order phase transition between two planar spin configurations characterized by $\phi = 0.5296$ and $\phi_M = 2.0111$, respectively. The magnetic field at which the first-order phase transition occurs is $h = 1.357\,53$. Note that the minima of $e_G^{(P)}$ are very near to those of $\Delta^{(P)}(1.357\,53, \phi)$ occurring at $\phi_0 = 0.4694$ and $\phi = \phi_M$ while the minimum of $e_0(1.35753, \phi)$ occurs at $\phi_m = 1.2619$. For increasing field the scenario is confirmed and the spin configuration is selected by quantum fluctuations. The minimum of $e_G^{(P)}$ locks at $\phi = \phi_M$.

In table 2 we give $e_G^{(U)}$ defined by equation (4.11), $e_G^{(U)}(j \to 0)$ defined by equation (4.15) and $e_G^{(P)}$ defined by equation (4.19) evaluated for the value of ϕ for which $e_G^{(P)}$ is a minimum. We have evaluated the second column of values to allow a homogeneous comparison between the ground-state energies of the U and P phases since the zero-point-motion energy for the P phase can be evaluated only in the limit where $j = 0$. As one can see by comparison of the second and third columns of table 2, the P phase replaces the U phase for any value of h. The comparison of the first and third columns leads one to the same conclusion but it is less reliable because the P phase would get an advantage from the 2D calculation as shown by the first row of table 2. Indeed the zero-point-motion energy lowers the ground-state energy as the number of dimensions decreases.

For compounds like VBr_2 and VCl_2 the realistic values of h are in the range $0 < h < 0.1$ corresponding to fields $0 < H < 10$ T, so the significant figure is figure 5. In this range one can perform an expansion of $\Delta^{(P)}(h, \phi)$ given by equation (4.20) in powers of h, obtaining

$$\Delta^{(P)}(h, \phi) = c_0 + c_2^{(P)} h^2 + c_3^{(P)} h^3 \cos(3\phi) + \cdots \tag{4.27}$$

where $c_0 = 2.344\,764$, $c_2^{(P)} = 0.142$, $c_3^{(P)} = 0.053$. The ground-state energy $e_G^{(P)}$ given in equation (4.19) evaluated for $\phi = \phi_m$ (see equation (4.26)) reads

$$e_G^{(P)}(\phi_m) = -\frac{3}{2} - \frac{1}{2}h^2 - j\left(1 - \frac{4}{9}h^2 - \frac{4}{81}h^4 + \cdots\right) - \frac{3}{2S} + \frac{1}{2S}\left(c_0 + c_2^{(P)} h^2 - 2c_3^{(P)} h^4 + \cdots\right). \tag{4.28}$$

Table 2. A comparison of the quantum energies of the U phase ($e_G^{(U)}$), the U phase expanded for small j ($e_G^{(U)}(j \to 0)$) and the P phase ($e_G^{(P)}$) as functions of the external magnetic field for $j = 0.01$.

h	$e_G^{(U)}$	$e_G^{(U)}(j \to 0)$	$e_G^{(P)}$
0	−1.725 415	−1.728 412	−1.728 412
0.1	−1.729 735	−1.732 672	−1.732 918
0.2	−1.742 752	−1.745 562	−1.746 501
0.3	−1.764 581	−1.767 238	−1.769 306
0.4	−1.795 343	−1.797 836	−1.801 502
0.5	−1.835 154	−1.837 478	−1.843 359
0.6	−1.884 122	−1.886 276	−1.895 276
0.7	−1.942 344	−1.944 329	−1.957 692
0.8	−2.009 910	−2.011 728	−2.031 018
0.9	−2.086 901	−2.088 554	−2.115 766
1.0	−2.173 393	−2.174 883	−2.213 143
1.1	−2.269 452	−2.270 783	−2.302 577
1.2	−2.375 142	−2.376 319	−2.402 957
1.3	−2.490 523	−2.491 549	−2.513 865
1.4	−2.615 649	−2.616 527	−2.635 967
1.5	−2.750 573	−2.751 308	−2.769 100
1.6	−2.895 344	−2.895 940	−2.912 060
1.7	−3.050 010	−3.050 472	−3.064 927
1.8	−3.214 621	−3.214 952	−3.227 772
1.9	−3.389 222	−3.389 427	−3.400 660
2.0	−3.573 863	−3.573 948	−3.583 652
2.5	−4.649 670	−4.649 258	−4.652 512
2.6	−4.895 881	−4.895 402	−4.897 667
2.7	−5.152 714	−5.152 190	−5.153 597
2.8	−5.420 382	−5.419 849	−5.420 555
2.9	−5.699 250	−5.698 776	−5.698 983
3.0	−5.990 162	−5.990 000	−5.990 000
3.013 33	−6.030 000	—	—

In the same range of parameters the ground-state energy of the U phase given by equation (4.15) reads

$$e_G^{(U)}(j \to 0) = -\frac{3}{2} - \frac{1}{2}h^2 - j\left(1 - \frac{2}{9}h^2\right) - \frac{3}{2S} + \frac{1}{2S}\left(c_0 + c_2^{(U)}h^2 - c_3^{(U)}h^3 + \ldots\right) \tag{4.29}$$

where $c_0 = 2.344\,764$, $c_2^{(U)} = 0.224$, $c_3^{(U)} = 0.092$. This allows us to show analytically the stability of the P phase. Indeed one has

$$\Delta e_G = e_G^{(U)}(j \to 0) - e_G^{(P)}(\phi_m) = \left[-\frac{2}{9}j + \frac{c_2^{(U)} - c_2^{(P)}}{2S}\right]h^2. \tag{4.30}$$

For $j = 0.01$ and $S = 3/2$ we obtain $\Delta e_G = 0.0251h^2$.

The small uniaxial anisotropy that one observes in VBr_2 [2] does not change the above conclusion but it selects the plane of the spins which is forced to contain both the c axis and the external magnetic field. Taking advantage of the small value of the single-ion anisotropy one can keep the zero-point-motion energy of the isotropic model and investigate its effect on the classical energies expanded for small h and d as given in equations (2.5) and (2.8).

We have

$$\Delta e_1 = e_0^{(\mathrm{U1})} - e_0^{(\mathrm{P})} + \frac{\Delta^{(\mathrm{U})} - \Delta^{(\mathrm{P})}}{2S} = \left[-\frac{2j(2j-|d|)}{9(2j+|d|)} \left(1 + \frac{3|d|}{4j}\right)^2 + \frac{0.041}{S} \right] h^2 \qquad (4.31)$$

and

$$\Delta e_2 = e_0^{(\mathrm{U2})} - e_0^{(\mathrm{P})} + \frac{\Delta^{(\mathrm{U})} - \Delta^{(\mathrm{P})}}{2S} = \frac{|d|^3}{3(9-d^2)} + \left[-\frac{2}{9} j \left(1 + \frac{|d|}{2j} - \frac{7d^2}{16j^2}\right) + \frac{0.041}{S} \right] h^2. \qquad (4.32)$$

For $S = 3/2$, $|d| = 0.003$, $j = 0.01$ we obtain $\Delta e_1 \simeq \Delta e_2 \simeq 0.0249h^2$ in good agreement with the result of equation (4.30). We stress the crucial role of quantum fluctuations in stabilizing the P phase.

The zero-point motion and spin reduction for some BX_2 compounds with uniaxial anisotropy were recently evaluated in zero field [14] by an approach very similar to ours.

Table 3. Bragg peak intensities for the U phase and the P phase at low magnetic field. Note that for BX_2 one has $j \simeq 0.01$, $h \simeq 0.01H$ (T). $R = 1/(1 + (3a/4c)^2) = 0.829$ for $a = 3.75$ Å and $c = 6.20$ Å.

	U phase	P phase
$I(0,0,1)$	$\dfrac{9h^2}{(9+4j)^2}$	$\dfrac{9h^2}{(9+8j)2}$
$I(\frac{1}{3}, \frac{1}{3}, \frac{1}{2})$	$\dfrac{1+R}{4}\left[1 - \dfrac{9h^2}{(9+4j)^2}\right]$	$\dfrac{1}{4}\left[1 - \dfrac{16jh^2}{(9+8j)^2}\right] - R\dfrac{(9-8j)h^2}{(9+8j)^2}$
$I(\frac{1}{3}, \frac{1}{3}, 0)$	0	$\dfrac{9h^2}{4(9+8j)^2}$
$I(0, 0, \frac{1}{2})$	0	0

5. The elastic neutron scattering cross section

Elastic neutron scattering experiments provide a suitable test for investigating whether the spin configuration is a U or a P configuration. By use of equation (3.1) of [10] we are able to give the intensity of the main Bragg peaks for the U and P configuration. In order to compare our theoretical results with the experimental data on elastic neutron scattering by VBr_2 [2], we consider the magnetic field along $(1, \bar{1}, 0)$—that is, our y axis. In table 3 we give the intensities of some Bragg peaks for a single-crystal monodomain spin configuration in the limit of small h ($h \simeq 0.01H$ (T) for BX_2). As one can see, the main difference between the U and P phases is seen by looking at the intensity of the peak at $(\frac{1}{3}, \frac{1}{3}, 0)$, which is zero in the U phase and proportional to the square of the magnetic field in the P phase. However, the sample of VBr_2 [2] was a single crystal with a multidomain magnetic configuration, so the Bragg peak intensities are to be compared with a suitable average over the magnetic domain distribution. A 120° three-sublattice spin pattern with the spins lying in planes containing the c axis, and with the uniform distribution of the magnetic domains around the c axis, fits the experimental data satisfactorily as shown in figure 5 of [2]. Under this hypothesis, the Bragg peak intensity at zero field, for m, n integers that are not multiples of 3 and 2, respectively, reads

$$I\left(\frac{m}{3}, \frac{m}{3}, \frac{n}{2}\right) = \frac{1}{4}\left(1 + \frac{1}{2}R_{m,n}\right) \qquad (5.1)$$

where

$$R_{m,n} = \frac{1}{1 + (3na/4mc)^2} \tag{5.2}$$

with $a = 3.75$ Å and $c = 6.20$ Å.

The application of an external magnetic field perpendicular to the c axis drives the system towards a homogeneous magnetic configuration. In the experiment [2] a magnetic field of up to 1.5 T was applied. The intensity of the Bragg peaks diminished with increasing field. This suggests that the system is driven towards a homogeneous configuration where the spins lie in a plane containing the c axis and the magnetic field (our yz plane). Indeed the intensity of the peaks (5.1) when an external magnetic field is applied along the y axis, is

$$I\left(\frac{m}{3}, \frac{m}{3}, \frac{n}{2}\right) = \frac{1}{4} \tag{5.3}$$

when the spins lie in a plane containing the c axis and the magnetic field. Note that this configuration is a P configuration. When the spins lie in the plane containing the c axis perpendicular to the field direction (the xz plane)—that is, a U configuration—the Bragg peak intensity reads

$$I\left(\frac{m}{3}, \frac{m}{3}, \frac{n}{2}\right) = \frac{1}{4}\left(1 + R_{m,n}\right). \tag{5.4}$$

The decrease of the peak intensities observed experimentally (see figure 2 of [2]) when the multidomain configuration is still present suggests an evolution of the spin structure towards a planar homogeneous spin configuration for which the peak intensities are given by (5.3), whereas an umbrella configuration would produce an enhanced intensity as given by (5.4). We suggest that elastic neutron scattering in a higher magnetic field would unambiguously test our theoretical expectation of a planar spin configuration supported by quantum fluctuations. Note that for a homogeneous spin configuration the field dependence of the peak intensity would be h^2 like. Indeed the observed h-dependence is due to an extrinsic phenomenon such as the domain rotation [2]. Moreover the presence of a Bragg peak at $(\frac{1}{3}, \frac{1}{3}, 0)$ is the signature of the P phase once a homogeneous magnetic configuration is obtained in a high enough magnetic field.

6. Summary and conclusions

In this paper we have studied the quantum fluctuations in the hexagonal antiferromagnet (HAF) in the limit of small interplane coupling and small single-ion easy-axis anisotropy, a model which is suitable for BX_2 compounds. The phase diagram in the classical approximation was obtained in section 2 and shown in figure 2 for an external magnetic field applied perpendicular to the c axis. We have found that quantum fluctuations play a crucial role. Indeed the minimum-energy spin configuration expected on the basis of the classical approximation for $d = 0$ is an umbrella (U) phase with its axis parallel to the magnetic field direction, but the zero-point-motion energy stabilizes a planar (P) configuration with the spins lying in a plane containing the magnetic field. This is shown in tables 1 and 2 for a set of Hamiltonian parameters suitable for some vanadium halides like VBr_2 and VCl_2 [2]. The scenario is reminiscent of the interesting phenomenology found in the isotropic triangular antiferromagnet (TAF) where the umbrella configuration has the same energy as infinite inequivalent planar configurations, when the classical approximation is used. In the isotropic TAF model, quantum fluctuations stabilize a planar spin configuration with one spin over three opposite to the field [7]. Even if a small single-ion easy-axis anisotropy

is present the minimum of the classical energy of the HAF model corresponds to the U phase, but a quasi-degeneracy with a P configuration survives, so the zero-point motion is crucial to the selection of the ground-state configuration. Indeed the difference between the classical energies of the U and P phases is of order $-J_{\parallel}H^2$ whereas the difference between the zero-point-motion energies of the U and P phases is of order $+J_{\perp}H^2/S$, as was shown in section 4. BX_2 compounds are systems where the phenomenology that we have studied may be tested. This possibility is obviously excluded for ABX_3 compounds characterized by a strong intrachain antiferromagnetic coupling.

In order to evaluate the zero-point-motion energy in section 3 we have studied the magnon spectrum energy of the HAF model. In section 4 we have studied the influence of quantum fluctuations on the ground state of the HAF model for $j = 0.01$ and $d = -0.003$, typical values for VBr_2 and VCl_2 [2]. We have found that the planar phase is stabilized by the zero-point motion for any external magnetic field up to the saturation magnetic field.

In section 5 we gave the elastic neutron scattering cross section (see table 3). We have found that the measurement of the intensity of the Bragg peak at $(\frac{1}{3}, \frac{1}{3}, 0)$ could be a good test to establish whether the spin configuration is U or P like. Indeed $I(\frac{1}{3}, \frac{1}{3}, 0)$ is zero in the former case, and proportional to the square of the field in the latter. We have re-examined the experimental data on the elastic neutron scattering from a single crystal of VBr_2 with a multidomain spin configuration [2] and we find that our expectation of a P phase in an external magnetic field supported by quantum fluctuations agrees with experiment.

Appendix A

In equation (3.4) the column matrix of boson operators $\mathbf{A}_{\boldsymbol{k}}$ is given by

$$\mathbf{A}_{\boldsymbol{k}} = \begin{pmatrix} a_{\boldsymbol{k}}^{(1)} \\ a_{\boldsymbol{k}}^{(2)} \\ a_{\boldsymbol{k}}^{(3)} \\ a_{\boldsymbol{k}}^{(4)} \\ a_{\boldsymbol{k}}^{(5)} \\ a_{\boldsymbol{k}}^{(6)} \end{pmatrix}. \tag{A.1}$$

The matrices appearing in (3.4) are given by

$$\mathbf{H}(\boldsymbol{k}) = \begin{pmatrix} H_{11} & H_{12}(\boldsymbol{k}) & H_{13}(\boldsymbol{k}) & H_{14}(\boldsymbol{k}) & 0 & 0 \\ H_{12}^*(\boldsymbol{k}) & H_{22} & H_{23}(\boldsymbol{k}) & 0 & H_{25}(\boldsymbol{k}) & 0 \\ H_{13}^*(\boldsymbol{k}) & H_{23}^*(\boldsymbol{k}) & H_{33} & 0 & 0 & H_{36}(\boldsymbol{k}) \\ H_{14}^*(\boldsymbol{k}) & 0 & 0 & H_{44} & H_{45}(\boldsymbol{k}) & H_{46}(\boldsymbol{k}) \\ 0 & H_{25}^*(\boldsymbol{k}) & 0 & H_{45}^*(\boldsymbol{k}) & H_{55} & H_{56}(\boldsymbol{k}) \\ 0 & 0 & H_{36}^*(\boldsymbol{k}) & H_{46}^*(\boldsymbol{k}) & H_{56}^*(\boldsymbol{k}) & H_{66} \end{pmatrix} \tag{A.2}$$

(A.3)

$$\mathbf{M}(\boldsymbol{k}) = \begin{pmatrix} M_{11} & M_{12}(\boldsymbol{k}) & M_{13}(\boldsymbol{k}) & M_{14}(\boldsymbol{k}) & 0 & 0 \\ M_{12}(-\boldsymbol{k}) & M_{22} & M_{23}(\boldsymbol{k}) & 0 & M_{25}(\boldsymbol{k}) & 0 \\ M_{13}(-\boldsymbol{k}) & M_{23}(-\boldsymbol{k}) & M_{33} & 0 & 0 & M_{36}(\boldsymbol{k}) \\ M_{14}(-\boldsymbol{k}) & 0 & 0 & M_{44} & M_{45}(\boldsymbol{k}) & M_{46}(\boldsymbol{k}) \\ 0 & M_{25}(-\boldsymbol{k}) & 0 & M_{45}(-\boldsymbol{k}) & M_{55} & M_{56}(\boldsymbol{k}) \\ 0 & 0 & M_{36}(-\boldsymbol{k}) & M_{46}(-\boldsymbol{k}) & M_{56}(-\boldsymbol{k}) & M_{66} \end{pmatrix}. \tag{A.4}$$

The matrix elements of (A.2) are

$$H_{11} = \frac{1}{2}g\mu_B H \sin\theta_1 \cos\phi_1 + \frac{1}{2}DS\big(1 - 3\cos^2\theta_1\big) - 3J_{\perp}S\big(r_{12} + r_{31}\big) - 2J_{\parallel}Sr_{14} \tag{A.5}$$

$$H_{12}(\boldsymbol{k}) = 3J_\perp S\,\frac{1}{2}h^*_{12}\gamma_{\boldsymbol{k}} \tag{A.6}$$

$$H_{13}(\boldsymbol{k}) = 3J_\perp S\,\frac{1}{2}h_{31}\gamma^*_{\boldsymbol{k}} \tag{A.7}$$

$$H_{14}(\boldsymbol{k}) = 2J_\parallel S\,\frac{1}{2}h^*_{14}\cos(ck_z) \tag{A.8}$$

$$H_{22} = \frac{1}{2}g\mu_B H\sin\theta_2\cos\phi_2 + \frac{1}{2}DS\big(1-3\cos^2\theta_2\big) - 3J_\perp S\big(r_{23}+r_{12}\big) - 2J_\parallel S r_{25} \tag{A.9}$$

$$H_{23}(\boldsymbol{k}) = 3J_\perp S\,\frac{1}{2}h^*_{23}\gamma_{\boldsymbol{k}} \tag{A.10}$$

$$H_{25}(\boldsymbol{k}) = 2J_\parallel S\,\frac{1}{2}h^*_{25}\cos(ck_z) \tag{A.11}$$

$$H_{33} = \frac{1}{2}g\mu_B H\sin\theta_3\cos\phi_3 + \frac{1}{2}DS\big(1-3\cos^2\theta_3\big) - 3J_\perp S\big(r_{31}+r_{23}\big) - 2J_\parallel S r_{36} \tag{A.12}$$

$$H_{36}(\boldsymbol{k}) = 2J_\parallel S\,\frac{1}{2}h^*_{36}\cos(ck_z) \tag{A.13}$$

$$H_{44} = \frac{1}{2}g\mu_B H\sin\theta_4\cos\phi_4 + \frac{1}{2}DS\big(1-3\cos^2\theta_4\big) - 3J_\perp S\big(r_{45}+r_{64}\big) - 2J_\parallel S r_{14} \tag{A.14}$$

$$H_{45}(\boldsymbol{k}) = 3J_\perp S\,\frac{1}{2}h^*_{45}\gamma_{\boldsymbol{k}} \tag{A.15}$$

$$H_{46}(\boldsymbol{k}) = 3J_\perp S\,\frac{1}{2}h_{64}\gamma^*_{\boldsymbol{k}} \tag{A.16}$$

$$H_{55} = \frac{1}{2}g\mu_B H\sin\theta_5\cos\phi_5 + \frac{1}{2}DS\big(1-3\cos^2\theta_5\big) - 3J_\perp S\big(r_{56}+r_{45}\big) - 2J_\parallel S r_{25} \tag{A.17}$$

$$H_{56}(\boldsymbol{k}) = 3J_\perp S\,\frac{1}{2}h^*_{56}\gamma_{\boldsymbol{k}} \tag{A.18}$$

$$H_{66} = \frac{1}{2}g\mu_B H\sin\theta_6\cos\phi_6 + \frac{1}{2}DS\big(1-3\cos^2\theta_6\big) - 3J_\perp S\big(r_{64}+r_{56}\big) - 2J_\parallel S r_{36}. \tag{A.19}$$

The matrix elements of (A.3) are

$$M_{11} = \frac{1}{2}DS\sin^2\theta_1 \tag{A.20}$$

$$M_{12}(\boldsymbol{k}) = 3J_\perp S\,\frac{1}{2}m_{12}\gamma_{\boldsymbol{k}} \tag{A.21}$$

$$M_{13}(\boldsymbol{k}) = 3J_\perp S\,\frac{1}{2}m_{31}\gamma^*_{\boldsymbol{k}} \tag{A.22}$$

$$M_{14}(\boldsymbol{k}) = 2J_\parallel S\,\frac{1}{2}m_{14}\cos(ck_z) \tag{A.23}$$

$$M_{22} = \frac{1}{2}DS\sin^2\theta_2 \tag{A.24}$$

$$M_{23}(\boldsymbol{k}) = 3J_\perp S\,\frac{1}{2}m_{23}\gamma_{\boldsymbol{k}} \tag{A.25}$$

$$M_{25}(\boldsymbol{k}) = 2J_\parallel S\,\frac{1}{2}m_{25}\cos(ck_z) \tag{A.26}$$

$$M_{33} = \frac{1}{2}DS\sin^2\theta_3 \tag{A.27}$$

$$M_{36}(\boldsymbol{k}) = 2J_\parallel S\,\frac{1}{2}m_{36}\cos(ck_z) \tag{A.28}$$

$$M_{44} = \frac{1}{2} DS \sin^2 \theta_4 \tag{A.29}$$

$$M_{45}(\boldsymbol{k}) = 3J_\perp S \frac{1}{2} m_{45} \gamma_{\boldsymbol{k}} \tag{A.30}$$

$$M_{46}(\boldsymbol{k}) = 3J_\perp S \frac{1}{2} m_{64} \gamma^*_{\boldsymbol{k}} \tag{A.31}$$

$$M_{55} = \frac{1}{2} DS \sin^2 \theta_5 \tag{A.32}$$

$$M_{56}(\boldsymbol{k}) = 3J_\perp S \frac{1}{2} m_{56} \gamma_{\boldsymbol{k}} \tag{A.33}$$

$$M_{66} = \frac{1}{2} DS \sin^2 \theta_6 \tag{A.34}$$

where

$$h_{ss'} = \sin\theta_s \sin\theta_{s'} + (1 + \cos\theta_s \cos\theta_{s'}) \cos(\phi_s - \phi_{s'}) + \mathrm{i}\,(\cos\theta_s + \cos\theta_{s'}) \sin(\phi_s - \phi_{s'}) \tag{A.35}$$

$$m_{ss'} = \sin\theta_s \sin\theta_{s'} - (1 - \cos\theta_s \cos\theta_{s'}) \cos(\phi_s - \phi_{s'}) - \mathrm{i}\,(\cos\theta_s - \cos\theta_{s'}) \sin(\phi_s - \phi_{s'}) \tag{A.36}$$

$$r_{ss'} = \sin\theta_s \sin\theta_{s'} \cos(\phi_s - \phi_{s'}) + \cos\theta_s \cos\theta_{s'} \tag{A.37}$$

$$\gamma_{\boldsymbol{k}} = \frac{1}{3} \left[\mathrm{e}^{\mathrm{i}ak_x} + 2\mathrm{e}^{-\frac{1}{2}\mathrm{i}ak_x} \cos\left(\frac{\sqrt{3}}{2} a k_y \right) \right]. \tag{A.38}$$

References

[1] Achiwa N 1969 *J. Phys. Soc. Japan* **27** 561
[2] Kadowaki H, Ubukoshi K and Hirakawa K 1985 *J. Phys. Soc. Japan* **54** 363
[3] Haldane F D M 1983 *Phys. Rev. Lett.* **50** 1153
Affleck I K 1985 *Nucl. Phys.* B **257** 397
[4] Morra R M, Buyers V J, Armstrong R L and Hirakawa K 1988 *Phys. Rev.* B **38** 543
Kakurai K, Steiner M, Pynn R and Kjems J K 1991 *J. Phys.: Condens. Matter* **3** 715
Enderle M, Kakurai K, Clausen K N, Inami T, Tanaka H and Steiner M 1994 *Europhys. Lett.* **25** 717
[5] Ohyama T and Shiba H 1993 *J. Phys. Soc. Japan* **62** 3277; *J. Phys. Soc. Japan* 1994 **63** 3454
[6] Kawamura H 1984 *J. Phys. Soc. Japan* **53** 2452
Rastelli E, Tassi A, Pimpinelli A and Sedazzari S 1992 *Phys. Rev.* B **45** 7936
[7] Chubukov A V and Golosov D I 1991 *J. Phys.: Condens. Matter* **3** 69
[8] Palme W, Mertens F, Born O, Lüthi B and Schotte U 1990 *Solid State Commun.* **76** 873
[9] Rastelli E and Tassi A 1994 *Phys. Rev.* B **49** 9879
Jacobs A E, Nikuni T and Shiba H 1993 *J. Phys. Soc. Japan* **62** 4066
[10] Rastelli E and Tassi A 1994 *Phys. Rev.* B **50** 16 745
[11] Tanaka H, Teraoka S, Kakehashi E, Iio K and Nagata K 1988 *J. Phys. Soc. Japan* **57** 3979
[12] Plumer M L and Caillé A 1990 *Phys. Rev.* B **42** 10 388
[13] Rastelli E and Tassi A 1994 *Z. Phys.* B **94** 139
Note that a doubled value of c_0 was erroneously given in equation (3.11).
[14] Watabe Y, Suzuki T and Natsume Y 1995 *Phys. Rev.* B **52** 3400